Hindawi
Mathematical Problems in Engineering
Volume 2019, Article ID 1364657, 14 pages
https://doi.org/10.1155/2019/1364657

Research Article

Nonlinear Hybrid Multipoint Model of High-Speed Train with Traction/Braking Dynamic and Speed Estimation Law

Chao Jia,[1] **Hongze Xu**,[1] **and Longsheng Wang**[2]

[1]*School of Electronic and Information Engineering, Beijing Jiaotong University, Beijing, 100044, China*
[2]*Signal & Communication Research Institute, China Academy of Railway Sciences, Beijing, 100081, China*

Correspondence should be addressed to Chao Jia; 15111015@bjtu.edu.cn

Received 7 September 2018; Accepted 31 December 2018; Published 17 January 2019

Academic Editor: Jorge Rivera

This paper establishes a NHMPM (Nonlinear Hybrid Multipoint Model) for HST (High-Speed Train) with the traction/braking dynamic and speed estimation law. Firstly, a full-order flux observer is designed using regional pole assignment theory to calculate the electromagnetic torque. The traction and braking forces are obtained according to this electromagnetic torque. Then the basic running resistance force is reformulated by considering the aerodynamic drag distribution characteristics, and the nonlinear in-train coupling force is analyzed as well. Next, the NHMPM including integer variables of running status and car types is built, where an adaptive parameter estimation algorithm and a speed estimation law are proposed to estimate unknown resistance coefficients and train speed, respectively. The effectiveness of the proposed algorithm, law, and NHMPM is verified through numerical simulations last.

1. Introduction

HST can operate safely and efficiently mainly depending on the performance of ATO (Automatic Train Operation) system, and the accurate dynamic model is the first stepstone for designing ATO control law [1]; therefore, many researchers have paid more attention to it during the past few decades [2–13]. There are mainly two types of models: single-point model and multipoint model. The former model ignores in-train dynamics and considers the train as a single mass point [2], which is widely used in energy saving optimization [3], automatic driving [4], and precise stopping [5]. However, the train is connected by couplers to transmit large traction and braking force, and this nonlinear force has a strong effect on the longitudinal motion of HST [6]. Therefore, it is necessary to consider the in-train dynamics that leads to the latter one.

The multipoint model was first introduced in 1990 [7] and then several scholars began to research on it [8–11]. In [8], a longitudinal multipoint model was established, in which the couplers were modelled as nonlinear springs, and the aerodynamic drag was assumed to act on the first car only. Reference [9] proposed a longitudinal model for heavy-haul trains, which took the coupler system as a linear spring with damping to simplify the calculation, and the aerodynamic drag was processed in the same manner as [8]. Reference [10] proposed a single coordinate model to solve the problem that the in-train coupling force was difficult to measure and directly control. In [11], a hybrid integer train model that includes running status integer variable was proposed after piecewise linearization of the train running resistance force.

It is noted that in most existing work, the traction and braking force are treated as control variables; the dynamics of these two forces are ignored, and therefore, the actual dynamic characteristics of the train cannot be accurately reflected [12]. In a recent work, an attempt has been made in accounting for these two forces, where the traction and braking force are linked with the motor current by nonlinear relations and two single-point models about traction and braking dynamics are proposed, respectively, in [13]. It is worth noting that the traction motor is a high-order, strong coupling, multivariable nonlinear system, and a simply nonlinear function cannot describe the traction and braking dynamics comprehensively. In addition, the basic resistance force is obtained by DAVIS formula and the resistance coefficients are available in most existing works. Also, in order

to facilitate the design of the controller, the basic resistance force is linearized. However, the resistance coefficients are variable and unknown due to the change of the line condition and the external environment [14], and the aerodynamic drag is related not only to the speed and resistance coefficients of the train, but also to the location of the car in practice [15].

Furthermore, train speed is the premise of completing ATO control. However, the installation of speed sensors increases the system cost, reduces the reliability of the system, and is not suitable for operating in a harsh environment [16]. By contrast, speed sensorless technology can identify the motor speed from easily measured physical quantities (stator voltage or stator current, for example) [17] and the train speed is obtained through the linear relation between these two speeds. In recent years, full-order flux observer method has received the widespread attention [18–22]. Generally, in order to make the observer converge faster than the traction motor, the observer gain matrix is designed such that the poles of the observer are k times more than the motor model. Reference [18] presented a method to estimate the motor speed based on adaptive flux observer, and let $k = 1$, but it caused the system to be unstable in low-speed range. Thus, [19] linearized the observer at the equilibrium point and increased the speed term; the range of k that can guarantee the stability of the system was obtained using the Routh stability criterion. An adaptive speed identification scheme for induction motor based on the hyperstability theory was proposed and $k = 1.2$ was chosen in [20]. In [21], the adaptive speed estimation for IM was analyzed, the necessary and sufficient conditions for stability of the speed estimation system were derived as well. And, furthermore, a novel observer gain was designed to guarantee the stability over the whole speed range by Lyapunov theory in [22]. However, if the observer gain is designed by traditional exact pole assignment method, it will limit the damping speed, deteriorate robustness, and be hard to satisfy multiple performances in some practical applications [23], such as robotic arm movement model [24], uniform damping control of low-frequency oscillations in power system [25], aircraft carrier landing control system [26], and flexible buildings [27]. Therefore, circularly regional pole assignment can be adopted to design the observer gain, which can make the observer have more degrees of freedom.

In this paper, traction and braking dynamics are described in detail, the basic resistance force is reformulated by considering aerodynamic drag distribution characteristics, and the nonlinear in-train coupling force is analyzed as well; the NHMPM including integer variables of running status and car types (locomotives or carriages) is built. An adaptive parameter estimation algorithm and a speed estimated law are proposed to provide unknown resistance coefficients and train speed required in the model, respectively.

The rest of this paper is organized as follows. In Section 2, traction and braking dynamics are discussed. Section 3 reformulates the basic resistance force and analyzes the nonlinear in-train coupling force. In Section 4, integer variables are introduced to represent running status and car types, and the NHMPM is derived, where an adaptive parameter estimation algorithm and speed estimation law are proposed to provide unknown resistance coefficients and train speed required in the model, respectively. Simulation is conducted in Section 5, and Section 6 draws the conclusion.

2. Traction and Braking Dynamics

2.1. Full-Order Flux Observer. The traction motor nominal model is described as the following equation in the stationary reference frame.

$$\begin{aligned}
&\dot{\boldsymbol{x}}_{\boldsymbol{s}} = \boldsymbol{A}_{\boldsymbol{m0}}\boldsymbol{x}_{\boldsymbol{s}} + \boldsymbol{B}_{\boldsymbol{m}}\boldsymbol{u}_{\boldsymbol{s}},\\
&\boldsymbol{y}_{\boldsymbol{s}} = \boldsymbol{i}_{\boldsymbol{s}} = \boldsymbol{C}_{\boldsymbol{m}}\boldsymbol{x}_{\boldsymbol{s}}.\\
&\boldsymbol{A}_{\boldsymbol{m}_0}\\
&\quad = \begin{bmatrix} -\lambda\left(R_{s0}L_r + R_{r0}L_s\right)\boldsymbol{I} + \omega_{r0}\boldsymbol{J} & \lambda R_{r0}\boldsymbol{I} - \lambda L_r\omega_{r0}\boldsymbol{J} \\ -R_{s0}\boldsymbol{I} & \boldsymbol{0} \end{bmatrix}\\
&\quad = \begin{bmatrix} \boldsymbol{A}_{11} & \boldsymbol{A}_{12} \\ \boldsymbol{A}_{21} & \boldsymbol{0} \end{bmatrix} = \begin{bmatrix} a_{11}\boldsymbol{I} + a'_{11}\boldsymbol{J} & a_{12}\boldsymbol{I} + a'_{12}\boldsymbol{J} \\ a_{21}\boldsymbol{I} & \boldsymbol{0} \end{bmatrix},\\
&B_m = \begin{bmatrix} b_1\boldsymbol{I} \\ \boldsymbol{I} \end{bmatrix} = \begin{bmatrix} \lambda L_r\boldsymbol{I} \\ \boldsymbol{I} \end{bmatrix},\\
&C_m = \begin{bmatrix} \boldsymbol{I} & \boldsymbol{0} \end{bmatrix},\\
&\boldsymbol{I} = \begin{bmatrix} 1 & 0 \\ 0 & 1 \end{bmatrix},\\
&\boldsymbol{J} = \begin{bmatrix} 0 & -1 \\ 1 & 0 \end{bmatrix},\\
&\boldsymbol{0} = \begin{bmatrix} 0 & 0 \\ 0 & 0 \end{bmatrix}.
\end{aligned} \tag{1}$$

Here, $\boldsymbol{x}_{\boldsymbol{s}} = [\boldsymbol{i}_{\boldsymbol{s}} \ \ \boldsymbol{\psi}_{\boldsymbol{s}}]^T$; $\boldsymbol{i}_{\boldsymbol{s}} = [i_{s\alpha} \ \ i_{s\beta}]^T$ is stator current; $\boldsymbol{\psi}_{\boldsymbol{s}} = [\psi_{s\alpha} \ \ \psi_{s\beta}]^T$ is stator flux; $\boldsymbol{u}_{\boldsymbol{s}} = [u_{s\alpha} \ \ u_{s\beta}]^T$ is stator voltage; R_s is stator resistance; R_r is rotor resistance; L_s is stator inductance; L_r is rotor inductance; L_m is mutual inductance; $\lambda = 1/(L_sL_r - L_m^2)$; ω_r is motor angular speed.

2.2. Observer Gain Matrix

Definition 1. For the sake of simplicity, let us introduce the following notations.

$$\begin{aligned}
\boldsymbol{A}_{\boldsymbol{ma}} &= \frac{\left(\boldsymbol{A}_{\boldsymbol{m0}} - c\boldsymbol{I}\right)}{r},\\
\boldsymbol{C}_{\boldsymbol{mr}} &= \frac{\boldsymbol{C}_{\boldsymbol{m}}}{r}.
\end{aligned} \tag{2}$$

$$\boldsymbol{A}_{\boldsymbol{mae}} = \frac{\left(\boldsymbol{A}_{\boldsymbol{m0}} + \boldsymbol{G}\boldsymbol{C}_{\boldsymbol{m}} - c\boldsymbol{I}\right)}{r}. \tag{3}$$

Here, $(c, 0)$ is the center of $D(c, r)$ and r is radius of $D(c, r)$ as shown in Figure 1. $\boldsymbol{G}$ is observer gain matrix.

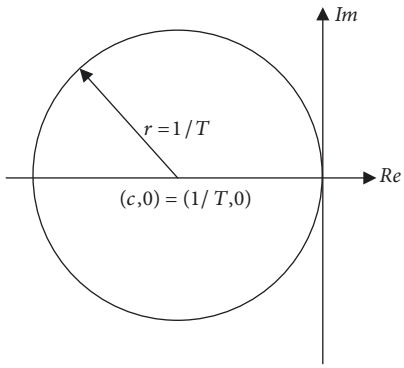

Figure 1: Circular region $D(c, r)$.

Take $\hat{\boldsymbol{x}}_s = [\hat{\boldsymbol{i}}_s \ \ \hat{\boldsymbol{\psi}}_s]^T$ as the state variable of the observer; the full-order flux observer of traction motor can be written as

$$\dot{\hat{\boldsymbol{x}}}_s = \boldsymbol{A}_{m0}\hat{\boldsymbol{x}}_s + \boldsymbol{B}_m\boldsymbol{u}_s + \boldsymbol{G}\left(\hat{\boldsymbol{y}}_s - \boldsymbol{y}_s\right) \tag{4}$$

where "$\hat{\ }$" denotes observed quantities; $\hat{\boldsymbol{y}}_s = \hat{\boldsymbol{i}}_s = \boldsymbol{C}_m\hat{\boldsymbol{x}}_s$. Using (1) and (4), the actual state estimation error system is

$$\dot{\boldsymbol{e}} = \left(\boldsymbol{A}_{m0} + \boldsymbol{G}\boldsymbol{C}_m\right)\boldsymbol{e}. \tag{5}$$

Here, $\boldsymbol{e} = \hat{\boldsymbol{x}}_s - \boldsymbol{x}_s$.$\boldsymbol{G}$ is designed such that all the poles of the observer are assigned in circular region $D(c, r)$; the circular region can be expressed as

$$\left(k_{max}\sigma_i + \frac{1}{T}\right)^2 + \left(k_{max}\Omega_i\right)^2 \le \left(\frac{1}{T}\right)^2. \tag{6}$$

Here, σ_i, Ω_i are the real part and the imaginary part of the i_{th} pole of the motor model, and they satisfy

$$s_i = \left\{\sigma_i + j\Omega_i \mid \Omega_i = \max\left(\left|\Omega_1\right|, \left|\Omega_3\right|\right)\right\}, \quad i = 1, 3. \tag{7}$$

T is the sampling period, and it satisfies the following inequality.

$$T \le T_c \le \frac{-2\sigma_i}{{\sigma_i}^2 + {\Omega_i}^2}. \tag{8}$$

And $k_{\max} = -2\sigma_i/T_c({\sigma_i}^2 + {\Omega_i}^2)$.

Theorem 2. *Let $\boldsymbol{R}$ be a positive definite symmetric matrix of appropriate dimensions. All the eigenvalues of $\boldsymbol{A}_{m0} + \boldsymbol{G}\boldsymbol{C}_m$ belong to $D(c, r)$ and the state estimation error system (5) is stable under an observer gain matrix $\boldsymbol{G}$ if and only if there exists a positive $\boldsymbol{P}$ satisfying the following inequality*

$$\begin{bmatrix} -\boldsymbol{P} & \boldsymbol{P}\boldsymbol{A}_{ma} \\ \boldsymbol{A}_{ma}^T\boldsymbol{P} & -\boldsymbol{P} - \boldsymbol{C}_{mr}^T\boldsymbol{R}^{-1}\boldsymbol{C}_{mr} \end{bmatrix} < 0. \tag{9}$$

Then the observer gain matrix $\boldsymbol{G}$ is given by

$$\boldsymbol{G} = -\boldsymbol{A}_{ma}\left(\boldsymbol{P} + \boldsymbol{C}_{mr}^T\boldsymbol{R}^{-1}\boldsymbol{C}_{mr}\right)^{-1}\boldsymbol{C}_{mr}^T\boldsymbol{R}^{-1}. \tag{10}$$

Proof. By Schur Complement Lemma in [28], (9) implies

$$\boldsymbol{P}\boldsymbol{A}_{ma}\left(\boldsymbol{P} + \boldsymbol{C}_{mr}^T\boldsymbol{R}^{-1}\boldsymbol{C}_{mr}\right)^{-1}\boldsymbol{A}_{ma}^T\boldsymbol{P} - \boldsymbol{P} < 0. \tag{11}$$

Multiplying $\boldsymbol{P}^{-1}$ by both sides of inequality (11), we can get

$$\boldsymbol{A}_{ma}\left(\boldsymbol{P} + \boldsymbol{C}_{mr}^T\boldsymbol{R}^{-1}\boldsymbol{C}_{mr}\right)^{-1}\boldsymbol{A}_{ma}^T - \boldsymbol{P}^{-1} < 0. \tag{12}$$

And there exists a positive definite symmetric matrix $\boldsymbol{Q}$ such that

$$\boldsymbol{A}_{ma}\left(\boldsymbol{P} + \boldsymbol{C}_{mr}^T\boldsymbol{R}^{-1}\boldsymbol{C}_{mr}\right)^{-1}\boldsymbol{A}_{ma}^T - \boldsymbol{P}^{-1} + \boldsymbol{Q} = 0. \tag{13}$$

Let

$$\boldsymbol{V} = \boldsymbol{A}_{mae}\boldsymbol{P}^{-1}\boldsymbol{A}_{mae}^T - \boldsymbol{P}^{-1}. \tag{14}$$

According to (13), we have

$$\boldsymbol{P}^{-1} = \boldsymbol{A}_{ma}\left(\boldsymbol{P} + \boldsymbol{C}_{mr}^T\boldsymbol{R}^{-1}\boldsymbol{C}_{mr}\right)^{-1}\boldsymbol{A}_{ma}^T + \boldsymbol{Q}. \tag{15}$$

Substituting (15) into (14) leads to

$$\begin{aligned}\boldsymbol{V} = {} & \boldsymbol{A}_{mae}\boldsymbol{P}^{-1}\boldsymbol{A}_{mae}^T - \boldsymbol{A}_{ma}\left(\boldsymbol{P} + \boldsymbol{C}_{mr}^T\boldsymbol{R}^{-1}\boldsymbol{C}_{mr}\right)^{-1}\boldsymbol{A}_{ma}^T \\ & - \boldsymbol{Q}.\end{aligned} \tag{16}$$

Now denote $\boldsymbol{U} = \boldsymbol{A}_{ma}(\boldsymbol{P} + \boldsymbol{C}_{mr}^T\boldsymbol{R}^{-1}\boldsymbol{C}_{mr})^{-1}$ and notice that

$$\begin{aligned}&\boldsymbol{A}_{ma}\left(\boldsymbol{P} + \boldsymbol{C}_{mr}^T\boldsymbol{R}^{-1}\boldsymbol{C}_{mr}\right)^{-1}\boldsymbol{A}_{ma}^T \\ &\quad = \boldsymbol{U}\boldsymbol{C}_{mr}^T\boldsymbol{R}^{-1}\boldsymbol{C}_{mr}\boldsymbol{U}^T + \boldsymbol{U}\boldsymbol{P}\boldsymbol{U}^T.\end{aligned} \tag{17}$$

Equation (16) is now given by

$$\boldsymbol{V} = \boldsymbol{A}_{mae}\boldsymbol{P}^{-1}\boldsymbol{A}_{mae}^T - \boldsymbol{U}\boldsymbol{C}_{mr}^T\boldsymbol{R}^{-1}\boldsymbol{C}_{mr}\boldsymbol{U}^T - \boldsymbol{U}\boldsymbol{P}\boldsymbol{U}^T - \boldsymbol{Q}. \tag{18}$$

When (19) is satisfied,

$$\begin{aligned}\boldsymbol{G} &= -\boldsymbol{A}_{ma}\left(\boldsymbol{P} + \boldsymbol{C}_{mr}^T\boldsymbol{R}^{-1}\boldsymbol{C}_{mr}\right)^{-1}\boldsymbol{C}_{mr}^T\boldsymbol{R}^{-1} \\ &= -\boldsymbol{U}\boldsymbol{C}_{mr}^T\boldsymbol{R}^{-1},\end{aligned} \tag{19}$$

we have

$$\boldsymbol{A}_{mae}\boldsymbol{P}^{-1}\boldsymbol{A}_{mae}^T = \boldsymbol{U}\boldsymbol{P}\boldsymbol{U}^T. \tag{20}$$

And then

$$\begin{aligned}\boldsymbol{V} &= \boldsymbol{U}\boldsymbol{P}\boldsymbol{U}^T - \boldsymbol{U}\boldsymbol{C}_{mr}^T\boldsymbol{R}^{-1}\boldsymbol{C}_{mr}\boldsymbol{U}^T - \boldsymbol{U}\boldsymbol{P}\boldsymbol{U}^T - \boldsymbol{Q} \\ &= -\boldsymbol{U}\boldsymbol{C}_{mr}^T\boldsymbol{R}^{-1}\boldsymbol{C}_{mr}\boldsymbol{U}^T - \boldsymbol{Q} = -\left(\boldsymbol{G}\boldsymbol{R}\boldsymbol{G}^T + \boldsymbol{Q}\right) < 0.\end{aligned} \tag{21}$$

That is,

$$\boldsymbol{V} = \boldsymbol{A}_{mae}\boldsymbol{P}^{-1}\boldsymbol{A}_{mae}^T - \boldsymbol{P}^{-1} < 0. \tag{22}$$

Or equivalently

$$\boldsymbol{A}_{mae}^T\boldsymbol{P}\boldsymbol{A}_{mae} - \boldsymbol{P} < 0. \tag{23}$$

That is, by Lemma 1 of [23], all the eigenvalues of $\boldsymbol{A}_{m0} + \boldsymbol{G}\boldsymbol{C}_m$ belong to $D(c, r)$, the error system is stable, and the proof is completed. □

Then the electromagnetic torque is obtained by the following equation.

$$T_e = n_p\left(\hat{\psi}_s^{\,T} J\, i_s\right) = n_p\left(\hat{\psi}_{s\beta} i_{s\alpha} - \hat{\psi}_{s\alpha} i_{s\beta}\right). \tag{24}$$

Here, n_p denotes the number of pole-pairs of traction motor; the electromagnetic torque is different when the train run in traction mode or braking mode, and we denote them as T_{et} and T_{eb}, respectively.

2.3. Traction Force and Braking Force. In this paper, we assume that the traction force and braking force of HST are all from the electromagnetic torque of traction motor, and they are linked with the motor stator voltage by a nonlinear relation. This nonlinear relation can be written as

$$\begin{aligned} F_{ti} &= \frac{2N_m a\eta}{D} T_{eti} = K_{ti} n_p\left(\hat{\psi}_{s\beta} i_{s\alpha} - \hat{\psi}_{s\alpha} i_{s\beta}\right) \\ &= K_{ti}\cdot h_t'\left(u_{si}\right), \\ F_{bi} &= \frac{2N_m a\eta}{D} T_{ebi} = K_{bi} n_p\left(\hat{\psi}_{s\beta} i_{s\alpha} - \hat{\psi}_{s\alpha} i_{s\beta}\right) \\ &= K_{bi}\cdot h_b'\left(u_{si}\right), \quad i = 1, 2, 3 \ldots p. \end{aligned} \tag{25}$$

Here, F_{ti}, F_{bi} are traction force and braking force of i_{th} car, respectively; N_m is the number of traction motors; a is gear ratio; η is transmission efficiency; p is the number of the locomotives; D is the diameter of half-worn wheel rolling circle.

3. Running Resistance Force and In-Train Coupling Force

In this section, the basic running resistance force is reformulated by analyzing the aerodynamic drag distribution characteristics, and the nonlinear in-train coupling force of each car is described simultaneously.

3.1. Running Resistance Force with Aerodynamic Resistance Distribution. The running resistance force f_{ri} of each car consists of the basic running resistance force f_{bi} and additional running resistance force f_{ai}; the empirical formula (DAVIS formula) is

$$\begin{aligned} f_{ri} &= f_{bi} + f_{ai} \\ &= \underbrace{m_i\left(c_0 + c_v v_i\right)}_{\text{rolling resistance force}} + \underbrace{m_i c_a v_i^2}_{\text{aerodynamic drag}} + f_{ai}, \\ & \qquad i = 1, 2, 3 \ldots n. \end{aligned} \tag{26}$$

Here, m_i, v_i are the mass and speed of the i_{th} car, respectively; c_0, c_v, c_a denote the resistance coefficients, which are related to the HST type; f_{ai} includes gradient, tunnel, and curve resistance force. The rolling resistance force is dominant in low-speed range and as the speed increases, the aerodynamic drag becomes dominant.

In fact, the aerodynamic drag consists of friction drag and pressure drag, which account for 24.7% and 75.3% of the total aerodynamic drag, respectively. Moreover, the aerodynamic drag of each car is not only related to its own mass and speed, but also related to the location of the car (the first car, the middle car, or the last car, for example) and whether to install air conditioning fairing, pantograph, and compartment connections, bogies, or other parts [15]. Therefore, the running resistance force can be reformulated as

$$f_{ri} = f_{bi} + f_{ai} = m_i\left(c_0 + c_v v_i\right) + k_{mi} M c_a v_i^2 + f_{ai}. \tag{27}$$

Here, M is the total mass of the train; k_{mi} is the percentage of aerodynamic drag of i_{th} car in the total aerodynamic drag.

Take CRH3 (China Railway High-Speed 3 series Electric Multiple Unit) as an example; the parameters of CRH3 are shown in Table 1. The basic running resistance force of each car is shown in Figure 2 when the speed varies from 0 m/s to 100 m/s (it is equivalent to the actual train speed from 0 km/h to 350 km/h). The dotted and solid lines represent the forces calculated by the first two items of (26) and (27), respectively.

In addition, the force deviation between these two formulas is shown in Figure 3. From Figure 3, we know that the basic running resistance force of each car has a large deviation before and after the formula modification, and the greater the speed, the larger the deviation. Moreover, the second car has the maximum deviation. Since the second and the seventh car are equipped with pantographs (see Figure 4), the pressure drag of these two cars is relatively greater than other cars

Table 1: The parameters of CRH3.

Symbol	Value	Unit
$m_1 - m_8$	67.2,69.6,68.8,63.2, 60.8,68.8,69.6,68	t
$k_1 - k_8$	16.1, 19.7, 7.5,9.6, 10.6,7.0,14.1,15.4	%
c_0, c_v, c_a	0.42,0.0016,0.000132	-

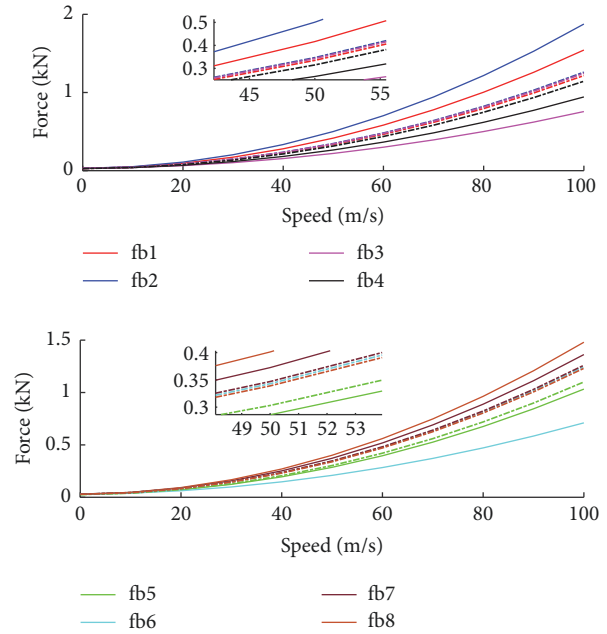

Figure 2: Basic running resistance force for CRH3.

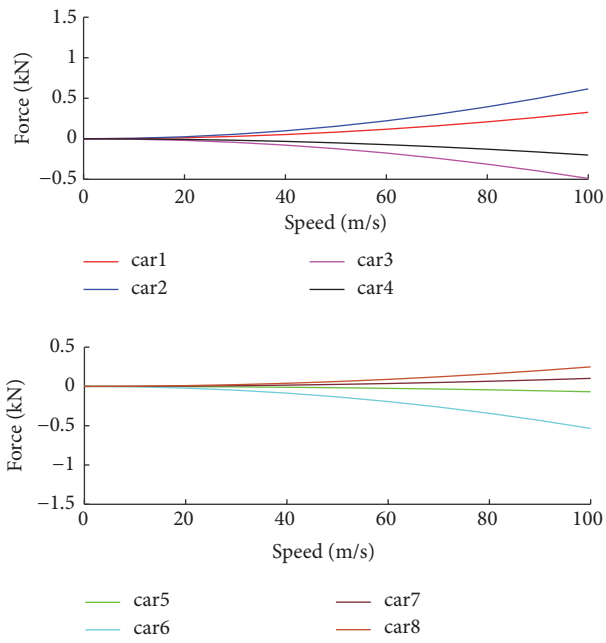

FIGURE 3: Basic running resistance force deviation between (26) and (27) of each car for CRH3.

without pantographs. Moreover, these two pantographs are installed opposite to each other, which results in two different wake flow fields; the intensity of the tail vortex induced by the second car's pantograph is stronger, which leads to the greater pressure drag than the seventh [15]. Thus, the second car has the largest aerodynamic drag and maximum deviation.

3.2. In-Train Coupling Force. A train is made up of many cars through springs; the coupling force is divided into two parts: spring part and damping part, and its dynamic equation can be written as

$$f_{in(i)(i+1)} = \underbrace{k_{si}\left(x_i - x_{i+1}\right)}_{spring\ part} + \underbrace{k_d\left(v_i - v_{i+1}\right)}_{damping\ part}. \tag{28}$$

Here, $f_{in(i)(i+1)}$ is the coupling force between the i_{th} car and the $(i+1)_{th}$ car; x_i, x_{i+1} are displacement of the i_{th} car and $(i+1)_{th}$ car, respectively; k_{si}, k_d are elastic coupling coefficient and damping coupling coefficient, respectively. k_{si} is the nonlinear function of displacement deviation, that is,

$$k_{si} = k_0\left[1 + \mu\left(x_i - x_{i+1}\right)^2\right] \quad i = 1, 2, \ldots, n-1. \tag{29}$$

Here, k_0 is constant; $\mu = 0$ denotes linear spring, that is, $k_{si} = k_0$, which does not exist in practice; $\mu < 0$ and $\mu > 0$ denote softening spring and hardening spring, respectively [8].

4. Nonlinear Multipoint Model of HST

In this section, NHMPM including integer variables of running status and car types is established, where an adaptive parameter estimation algorithm for estimating the unknown resistance coefficients is proposed and a train speed estimated law is derived to get train speed.

4.1. Nonlinear Hybrid Multipoint Model of HST. Take CRH3 as an example; it consists of four locomotives equipped with traction units (see Figure 4, the black wheels) and four carriages, and we define the output of traction units as u_e. Let $\gamma = 1$ and $\gamma = 0$ denote locomotives and carriages, respectively. In addition, we define "traction and cruise" states as "traction mode" because both of these two states require traction force; let $\delta = 1$ denote this mode; define "coasting" and "braking" states as "coast mode" and "braking mode"; let $\delta = 0$ and $\delta = -1$ denote these two modes, respectively. Therefore, the output of the execution unit of the i_{th} car is described as

$$u_{ei} = \frac{\gamma\left\{|\delta|\left(F_{ti} + F_{bi}\right) + \delta\left(F_{ti} - F_{bi}\right)\right\}}{2} = \frac{\gamma\left\{|\delta|\left[K_{ti}h_t'\left(u_{si}\right) + K_{bi}h_b'\left(u_{si}\right)\right] + \delta\left[K_{ti}h_t'\left(u_{si}\right) - K_{bi}h_b'\left(u_{si}\right)\right]\right\}}{2} \tag{30}$$
$$i = 1, 2, 3, \ldots, n;\ \delta = -1, 0, 1.$$

Now we assume that the displacement of each car is the same when the coupler is not stressed. The force analysis of the other cars is the same except the first and the last car which lack coupling force; the force analysis is shown for the fifth car in Figure 4. According to the Newton's second law, NHMPM can be expressed as (31).

$$\begin{aligned}
m_1\dot{v}_1 &= u_{e1} - f_{in12} - f_{r1} \\
&= \frac{\gamma\left\{|\delta|\left[K_{t1}h_t'\left(u_{s1}\right) + K_{b1}h_b'\left(u_{s1}\right)\right] + \delta\left[K_{t1}h_t'\left(u_{s1}\right) - K_{b1}h_b'\left(u_{s1}\right)\right]\right\}}{2} - k_0\left(x_1 - x_2\right) - k_0\mu\left(x_1 - x_2\right)^3 \\
&\quad - k_d\left(v_1 - v_2\right) - m_1\left(c_0 + c_v v_1\right) - k_{m1}Mc_a{v_1}^2 - f_{a1}, \\
m_i\dot{v}_i &= u_{ei} + f_{in(i-1)i} - f_{in(i)(i+1)} - f_{ri} \\
&= \frac{\gamma\left\{|\delta|\left[K_{ti}h_t'\left(u_{si}\right) + K_{bi}h_b'\left(u_{si}\right)\right] + \delta\left[K_{ti}h_t'\left(u_{si}\right) - K_{bi}h_b'\left(u_{si}\right)\right]\right\}}{2} + k_0\left(x_{i-1} - x_i\right) + k_0\mu\left(x_{i-1} - x_i\right)^3
\end{aligned}$$

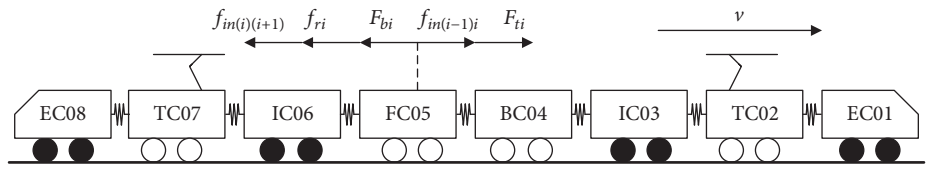

Figure 4: The framework of CRH3 series EMU and force analysis for one car.

$$+ k_d(v_{i-1} - v_i) - k_0(x_i - x_{i+1}) - k_0\mu(x_i - x_{i+1})^3 - k_d(v_i - v_{i+1}) - m_i(c_0 + c_v v_i) - k_{mi} M c_a {v_i}^2 - f_{ai},$$
$$(i = 2, 3, \ldots, n-1;)$$

$$m_n \dot{v}_n = u_{en} + f_{in(n-1)n} - f_{rn}$$
$$= \frac{\gamma\left\{|\delta|\left[K_{tn}h_t'(u_{sn}) + K_{bn}h_b'(u_{sn})\right] + \delta\left[K_{tn}h_t'(u_{sn}) - K_{bn}h_b'(u_{sn})\right]\right\}}{2} + k_0(x_{n-1} - x_n) + k_0\mu(x_{n-1} - x_n)^3$$
$$+ k_d(v_{n-1} - v_n) - m_n(c_0 + c_v v_n) - k_{mn} M c_a {v_n}^2 - f_{an} \quad (\gamma = 0, 1;\ \delta = -1, 0, 1)$$
$$\dot{x}_i = v_i \quad (i = 1, 2, 3, \ldots, n) \tag{31}$$

Sequentially, input variable $u \coloneqq [u_{s1}, u_{s2} \ldots u_{sn}]^T_{2n\times 1}$ and state variable $x \coloneqq [v_1, v_2 \ldots v_n, x_1, x_2 \ldots x_n]^T_{2n\times 1}$ are defined for transforming (31) to a nonlinear function form, where $u_{si} = [u_{s\alpha i}\ \ u_{s\beta i}]^T$ is traction motor stator voltage of the i_{th} car. In addition, the additional resistance force of the train is not easy to describe in a mathematical form such that it will be regarded as an unknown and bounded disturbance term d; furthermore the speed and displacement of the first car are taken as the output variable $y \coloneqq [v_1\ \ x_1]^T$. Therefore, (31) can be rewritten as the nonlinear function form.

$$\dot{x} = f'(x, u, d),$$
$$y = Cx. \tag{32}$$

Here, $C = \left[\begin{smallmatrix} 1\ 0 \ldots 0\ 0\ 0 \ldots 0 \\ 0\ 0 \ldots 0\ 1\ 0 \ldots 0 \end{smallmatrix}\right]_{2\times 2n}$.

4.2. Adaptive Parameter Estimation. Resistance coefficients are unknown and time varying, which will affect the accuracy of the model in practice. In this section, an adaptive parameter estimation algorithm is proposed to estimate these coefficients online for NHMPM, and the algorithm is based on the idea of [29].

The nonlinear model (32) is modified as the following form.

$$\dot{x} = f_0'(x, u, d) + C_0 + C_v x + C_a x^2. \tag{33}$$

Here, $K_m = \left[\begin{smallmatrix} k_{m1} & & & \\ & k_{m2} & & \\ & & \cdots & \\ & & & k_{mn} \end{smallmatrix}\right]$, $M_\Lambda = \left[\begin{smallmatrix} m_1 & & & \\ & m_2 & & \\ & & \cdots & \\ & & & m_n \end{smallmatrix}\right]$, $C_0 = \left[\begin{smallmatrix} C_0^p \\ 0_{n\times n} \end{smallmatrix}\right]$, $C_v = \left[\begin{smallmatrix} C_v^p & 0_{n\times n} \\ 0_{n\times n} & 0_{n\times n} \end{smallmatrix}\right]$, $C_a = \left[\begin{smallmatrix} (K_m M/M_\Lambda) C_a^p & 0_{n\times n} \\ 0_{n\times n} & 0_{n\times n} \end{smallmatrix}\right]$, $C_0^p = -[c_0\ \ c_0\ \ \ldots\ \ c_0]^T$, $C_v^p = -\mathrm{diag}(c_v, c_v, \ldots c_v)$, $C_a^p = -\mathrm{diag}(c_a, c_a, \ldots c_a)$.

Now, we define the following vector.

$$\mathrm{O} \coloneqq [C_0, C_v, C_a]^T. \tag{34}$$

$$\Phi \coloneqq \left[1, x, x^2\right]^T. \tag{35}$$

Then (33) can be rewritten as

$$\dot{x} = f_0'(x, u, d) + \Phi^T \mathrm{O}. \tag{36}$$

In order to simplify the adaptive parameter estimated algorithm and improve the engineering practicability, the resistance coefficients of each car are assumed to be equal as the train is in the same environment most of the time. Thus, we use the equivalent single-point model to estimate the resistance coefficients. It can be described as

$$\dot{v}_e = f_0''(u_s, d_0) + \varphi^T \theta \tag{37a}$$

$$\dot{x}_e = v_e. \tag{37b}$$

Here, d_0 is bounded disturbance term; $\varphi = [1, v_e, {v_e}^2]^T$; $\theta = [c_0, c_v, c_a]^T$, $\theta \in \mathbb{R}^{n\theta}$ is an unknown time-varying parameter. However, we can obtain a rough range from wind tunnel testing. In addition, we give the following assumptions.

Assumption 3. There exists an initially known nominal compact set $\Theta^0 \triangleq B(\theta^0, z_\theta^0)$, which is described by an initial nominal estimate θ^0 and associated error bound $z_\theta^0 = \sup_{s\in\Theta^0}\|s - \theta^0\|$ such that $\theta \in \Theta^0$.

Let the state predictor for (37a) be denoted as $\dot{\overline{v}}_e$ and define

$$\dot{\overline{v}}_e = f_0''(u_s, d_0) + \varphi^T \overline{\theta} + k_a e_v + y_\omega \dot{\overline{\theta}}. \tag{38}$$

Here, $\overline{\theta} \coloneqq [\overline{c}_0, \overline{c}_v, \overline{c}_a]^T$ is parameter estimate vector; $k_a > 0$ is constant matrix; $e_v = v_e - \overline{v}_e$ is prediction error; y_ω is the output of the filter and it can be expressed as

$$\dot{y}_\omega = \varphi - k_a y_\omega, \quad y_\omega(t_0) = 0. \tag{39}$$

Let $\tilde{\theta} = \theta - \overline{\theta}$; from (37a) and (38),

$$\dot{e}_v = \varphi^T \tilde{\theta} - k_a e_v - y_\omega \dot{\overline{\theta}}. \tag{40}$$

Define

$$\varsigma = e_v - y_\omega \tilde{\theta}. \tag{41}$$

From (40) and (41), we can get

$$\begin{aligned} \dot{\varsigma} &= -k_a \varsigma, \\ \varsigma(t_0) &= e_v(t_0). \end{aligned} \tag{42}$$

The adaptive estimation law of parameter $\overline{\theta}$ is given by (43).

$$\begin{aligned} \dot{\overline{\theta}} &= \kappa y_\omega^T (e_v - \varsigma), \\ \overline{\theta}(t_0) &= \theta^0 \end{aligned} \tag{43}$$

with $\kappa = \kappa^T > 0$.

Definition 4.

(1) $Y \in \mathbb{R}^{n_\theta \times n_\theta}$ is generated from

$$\begin{aligned} \dot{Y} &= y_\omega^T y_\omega, \\ Y(t_0) &= 0. \end{aligned} \tag{44}$$

(2) $\underline{\kappa} = \underline{\omega}(\kappa)$; excitation index $\varepsilon(t) = \underline{\omega}(Y(t))$; and contraction factor is

$$0 < \alpha(t) = \frac{1}{1 + \underline{\kappa}\varepsilon(t)} \leqslant 1. \tag{45}$$

The uncertainty set $\Theta \triangleq B(\overline{\theta}, z_\theta)$ is updated as the updating of the parameter estimate $\overline{\theta}$ and its associated error bound $z_\theta = \sup_{s\in\Theta} \|s - \overline{\theta}\|$. And z_θ is given as

$$z_\theta = z_\theta^\varepsilon = \sqrt{V_\varepsilon}. \tag{46}$$

Here, $V_\varepsilon(t) = \alpha(t) V_\varepsilon(t_0)$, $V_\varepsilon(t_0) = (1/2)(z_\theta^0)^2$.

Algorithm 5 (adaptive estimation algorithm of the parameter $\overline{\theta}$).

Step 1. Initialize k_a, φ, κ, θ^0, $v_e(t_0)$, $y_\omega(t_0)$, $\varsigma(t_0)$, *and* $z_\theta(t_0) = z_\theta^0$, $\overline{\theta}(t_0) = \overline{\theta}^0$, $\Theta^0 \triangleq B(\theta^0, z_\theta^0)$ at time t_0.

Step 2. Measure (or estimate, see Section 4.3) the current value of $v_e(t_i)$, and obtain y_ω, e_v, ς by (39)-(42).

Step 3. Update $\overline{\theta}(t_i)$ and $z_\theta(t_i)$ according to (43) and (46).

If the following conditions are met,

$$z_\theta(t_i) \leqslant z_\theta(t_{i-1}) - \left\| \overline{\theta}(t_i) - \overline{\theta}(t_{i-1}) \right\|. \tag{47}$$

Otherwise, keep the value of the last time, which is

$$\left(\overline{\theta}(t_i), z_\theta(t_i)\right) = \left(\overline{\theta}(t_{i-1}), z_\theta(t_{i-1})\right). \tag{48}$$

Step 4. Iterate back to Step 2, incrementing $i = i + 1$.

4.3. Train Speed Estimation. In this section, an adaptive speed estimated law for HST is proposed to get the train speed information instead of speed sensors.

Assumption 6. ω_{r0} is constant in the control period; that is, $d\omega_{r0}/dt = 0$.

In this paper, we assume that the motor parameters are constant except motor speed. Thus, the full-order flux observer of traction motor can be rewritten as

$$\begin{aligned} \dot{\hat{\boldsymbol{x}}}_s' &= \widehat{\boldsymbol{A}}_m \hat{\boldsymbol{x}}_s' + \boldsymbol{B}_m \boldsymbol{u}_s + \boldsymbol{G}\left(\hat{\boldsymbol{y}}_s' - \boldsymbol{y}_s\right) \\ &= \left(\boldsymbol{A}_{m0} + \Delta\boldsymbol{A}_m\right)\hat{\boldsymbol{x}}_s' + \boldsymbol{B}_m \boldsymbol{u}_s + \boldsymbol{G}\left(\hat{\boldsymbol{y}}_s' - \boldsymbol{y}_s\right) \\ \widehat{\boldsymbol{A}}_m &= \begin{bmatrix} \widehat{\boldsymbol{A}}_{11}' & \widehat{\boldsymbol{A}}_{12}' \\ \widehat{\boldsymbol{A}}_{21}' & \boldsymbol{0} \end{bmatrix} = \begin{bmatrix} a_{11}\boldsymbol{I} + \hat{a}_{11}'\boldsymbol{J} & a_{12}\boldsymbol{I} + \hat{a}_{12}'\boldsymbol{J} \\ a_{21}\boldsymbol{I} & \boldsymbol{0} \end{bmatrix} \\ &= \begin{bmatrix} -\lambda\left(R_{s0}L_r + R_{r0}L_s\right)\boldsymbol{I} + \hat{\omega}_r\boldsymbol{J} & \lambda R_{r0}\boldsymbol{I} - \lambda L_r\hat{\omega}_r\boldsymbol{J} \\ -R_{s0}\boldsymbol{I} & \boldsymbol{0} \end{bmatrix} \\ \Delta\boldsymbol{A}_m &= \begin{bmatrix} \Delta\omega_r\boldsymbol{J} & -b_1\Delta\omega_r\boldsymbol{J} \\ 0 & 0 \end{bmatrix} \end{aligned} \tag{49}$$

where $\hat{\boldsymbol{x}}_s' = [\hat{\boldsymbol{i}}_s' \;\; \hat{\boldsymbol{\psi}}_s']^T$; $\hat{\boldsymbol{y}}_s' = \hat{\boldsymbol{i}}_s' = \boldsymbol{C}_m\hat{\boldsymbol{x}}_s'$; $\Delta\omega_r = \hat{\omega}_r - \omega_{r0}$.

According to (49) and (1), the state estimation error system is

$$\dot{\boldsymbol{e}}_1 = \left(\boldsymbol{A}_{m0} + \boldsymbol{G}\boldsymbol{C}_m\right)\boldsymbol{e}_1 + \Delta\boldsymbol{A}_m\hat{\boldsymbol{x}}_s'. \tag{50}$$

Here, $\boldsymbol{e}_1 = \hat{\boldsymbol{x}}_s' - \boldsymbol{x}_s$.

Now we define a Lyapunov function candidate.

$$\boldsymbol{V}_1 = \boldsymbol{e}_1^T\boldsymbol{e}_1 + \frac{\left(\hat{\omega}_r - \omega_{r0}\right)^2}{\lambda_1}. \tag{51}$$

Here, λ_1 is a positive constant. The time derivative of V_1 by Assumption 6 becomes

$$\begin{aligned} \frac{d\boldsymbol{V}_1}{dt} &= \boldsymbol{e}_1^T\left[\left(\boldsymbol{A}_{m0} + \boldsymbol{G}\boldsymbol{C}_m\right)\boldsymbol{e}_1 + \Delta\boldsymbol{A}_m\hat{\boldsymbol{x}}_s'\right] \\ &\quad + \left[\left(\boldsymbol{A}_{m0} + \boldsymbol{G}\boldsymbol{C}_m\right)\boldsymbol{e}_1 + \Delta\boldsymbol{A}_m\hat{\boldsymbol{x}}_s'\right]^T\boldsymbol{e}_1 \\ &\quad + 2\frac{\Delta\omega_r}{\lambda_1}\frac{d\hat{\omega}_r}{dt} \\ &= \boldsymbol{e}_1^T\left[\left(\boldsymbol{A}_{m0} + \boldsymbol{G}\boldsymbol{C}_m\right)^T + \left(\boldsymbol{A}_{m0} + \boldsymbol{G}\boldsymbol{C}_m\right)\right]\boldsymbol{e}_1 \\ &\quad + 2\boldsymbol{e}_1^T\Delta\boldsymbol{A}_m\hat{\boldsymbol{x}}_s' + 2\frac{\Delta\omega_r}{\lambda_1}\frac{d\hat{\omega}_r}{dt} \\ &= \boldsymbol{e}_1^T\left[\left(\boldsymbol{A}_{m0} + \boldsymbol{G}\boldsymbol{C}_m\right)^T + \left(\boldsymbol{A}_{m0} + \boldsymbol{G}\boldsymbol{C}_m\right)\right]\boldsymbol{e}_1 \\ &\quad + 2\Delta\omega_r\left[\Delta\boldsymbol{i}_s'^T J\left(\hat{\boldsymbol{i}}_s' - b_1\hat{\boldsymbol{\psi}}_s'\right)\right] + 2\frac{\Delta\omega_r}{\lambda_1}\frac{d\hat{\omega}_r}{dt}. \end{aligned} \tag{52}$$

By Theorem 2, the first term on the right side of (52) is a seminegative matrix. When (53) is satisfied,

$$\frac{d\hat{\omega}_r}{dt} = \lambda_1\left[\Delta\boldsymbol{i}_s'^T J\left(b_1\hat{\boldsymbol{\psi}}_s' - \hat{\boldsymbol{i}}_s'\right)\right]. \tag{53}$$

Table 2: The simulation parameters.

Symbol	Value	Unit
U_d, U_L, P_m, f, n_p	3200, 2750, 560, 138, 2	$V, V, kW, Hz, -$
N_m, D, R_{s0}, R_{r0}	16, 0.875, 0.1065, 0.0663	$-, m, \Omega, \Omega$
$L_s, L_r, L_m, c_0, c_v, c_a,$	1.31, 1.93, 53.6, 0.42, 0.0016, 0.000132	$mH, mH, mH, -, -, -$
k_d, k_0, μ, a, η	$5 \times 10^6, 2 \times 10^7, -0.1,\ 2.788, 0.975$	$N{\cdot}s/m, N/m, -, -, -$
$k_1, k_2, k_3, m_1, m_2, m_3$	31.4, 38.5, 30.1, 67.2, 69.6, 68	%, %, %, t, t, t

The last two terms on the right side of (52) are equal, which leads to $d\boldsymbol{V}_1/dt \leq 0$. Therefore, it satisfies the Lyapunov stability law and guarantees the stability of the speed estimation system. And (53) is the angular speed identification adaptive law; then, PI adaptive law is adopted to satisfy the rapidity of identification, and it can be expressed as

$$\widehat{\omega}_r = \left(k_{wp} + k_{wI}\int dt\right)\left(\Delta \boldsymbol{i}_s'^{\boldsymbol{T}} J\left(b_1\widehat{\boldsymbol{\psi}}_s' - \widehat{\boldsymbol{i}}_s'\right)\right). \tag{54}$$

Here, k_{wp}, k_{wI} are PI parameters, respectively. Then HST speed is obtained by (55).

$$\begin{aligned}\widehat{v} &= \frac{60\pi D}{1000a}\cdot\frac{30}{\pi}\widehat{\omega}_r \\ &= \frac{1.8D}{a}\left(k_{wp} + k_{wI}\int dt\right)\left(\Delta \boldsymbol{i}_s'^{\boldsymbol{T}} J\left(b_1\widehat{\boldsymbol{\psi}}_s' - \widehat{\boldsymbol{i}}_s'\right)\right).\end{aligned} \tag{55}$$

Here, $\widehat{v}$ is the speed of HST.

5. Numerical Simulation

In this section, CRH3 is chosen for the simulation to verify the validity of speed estimation law, adaptive parameters estimation algorithm, and NHMPM. In order to simplify the simulation and not to lose the generality as well, three cars are chosen (the first and last are locomotives and the middle is carriage). The simulation parameters are shown in Table 2 [15, 16, 30, 31].

In Table 2, U_L is rated line voltage, P_m is rated power of traction motor, and f is rated frequency of traction motor.

The verification framework is shown in Figure 5, and the detailed process is as follows.

Firstly, the target speed (see black line in Figure 8) is given which is 15m/s (0-1s), 70 m/s (1-2s), 30 m/s (2-3s), 3 m/s (3-4s). The real speed (see blue line in Figure 8) and the stator current are measured by sensors after traction motor vector control. In addition, the estimated speed is obtained by (55) (see red line in Figure 8). Compare the estimated speed and real speed to verify the validity of the speed estimation law.

Secondly, according to measured stator current and observed stator flux by full-order flux observer, the electromagnetic torque is obtained by (24), so we can get traction force and braking force by (25) and these forces are also taken as input for TMPM (Traditional Multipoint Model).

Lastly, the calculated speed of NHMPM is obtained by (31). Compare the real speed and calculated speed to prove the validity of NHMPM. And determine whether the calculated speed of NHMPM is closer to the real speed than TMPM to verify the accuracy of NHMPM.

In addition, determine whether the resistance coefficients estimated by Algorithm 5 converge to the real values to verify the effectiveness of the adaptive parameter estimation algorithm.

5.1. The Validity of Speed Estimation Law. According to Table 2, we can get

$$A_{m0} = \begin{bmatrix} -54.23 & -650.31 & 380 & 2.0496\times10^5 \\ -650.31 & -54.23 & -2.0496\times10^5 & 380 \\ -0.1065 & 0 & 0 & 0 \\ 0 & -0.1065 & 0 & 0 \end{bmatrix}, \tag{56}$$

$$B_m = \begin{bmatrix} 315.167 & 0 \\ 0 & 315.167 \\ 1 & 0 \\ 0 & 1 \end{bmatrix}.$$

When $\omega_r = 1.5p.u.$, the poles of the motor model are $(-20.64+649.3i), (-20.64-649.3i), (-33.59-1.01i), (-33.59+1.01i)$. We can get $T \leq 9.78\times10^{-5}$ by (8); let $T = 9\times10^{-5}$ and then $k_{\max} = 1.08$. Therefore, the circular region $D(c, r)$ is obtained by (6) with center $(c, 0) = (-1/9\times10^5, 0)$ and $r = 1/9\times10^5$. Figure 6 shows the trajectories of observer poles when ω_r changes from 0 to$1.5p.u.$ and the circular region $D(c, r)$. From the figure, we know that all of the poles of observer belong to the circular region $D(c, r)$. The poles of the motor model and observer are shown in Figure 7 when $\omega_r = 1.5p.u.$

According to the simulation parameter, solving the linear matrix inequality (9), the feasible solution of $\boldsymbol{P}$ and observer gain matrix $\boldsymbol{G}$ are

$$\boldsymbol{P} = 10^{-6}\times\begin{bmatrix} 0.0065 & 0 & -2.0561 & -0.2392 \\ 0 & 0.0065 & 0.2392 & -2.0561 \\ -2.0561 & 0.2392 & 1832.8 & -2.87487\times10^{-9} \\ -0.2392 & -2.0561 & -2.87487\times10^{-9} & 1832.8 \end{bmatrix},$$

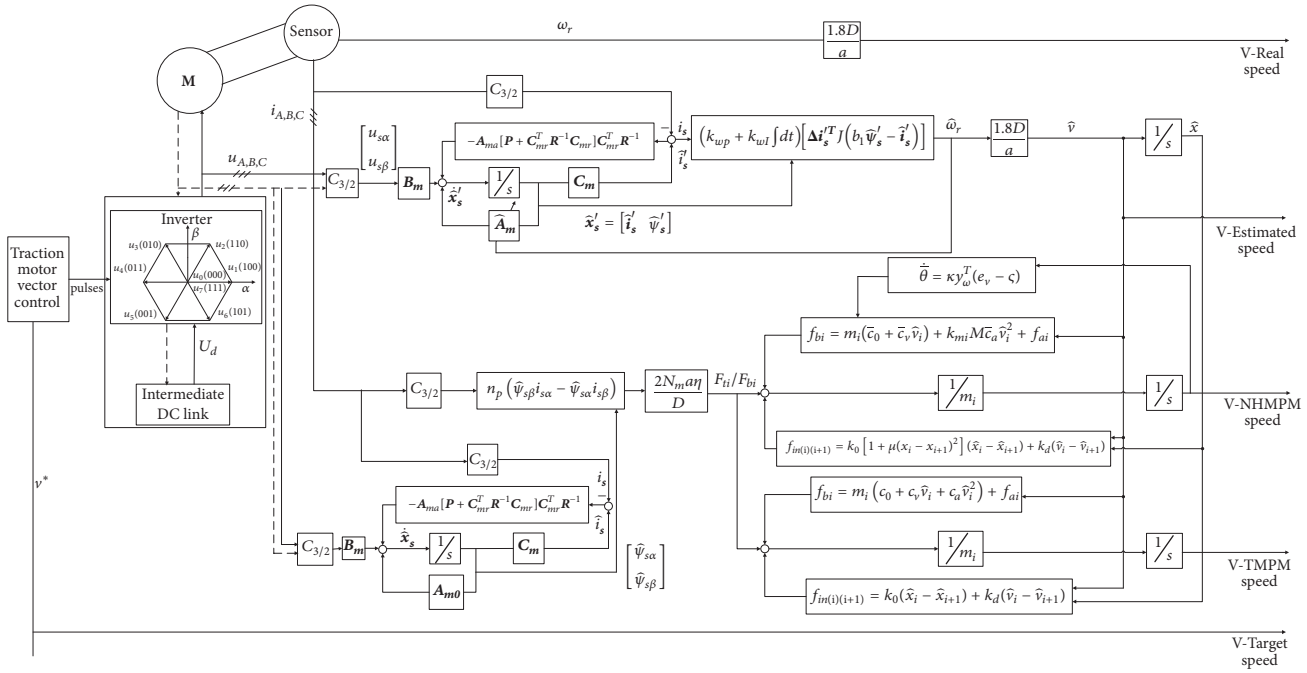

Figure 5: The verification framework.

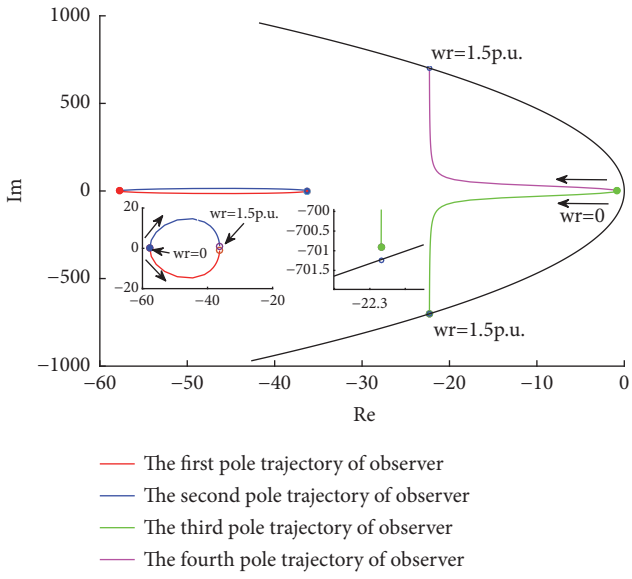

Figure 6: The trajectories of observer poles and circular region $D(c, r)$.

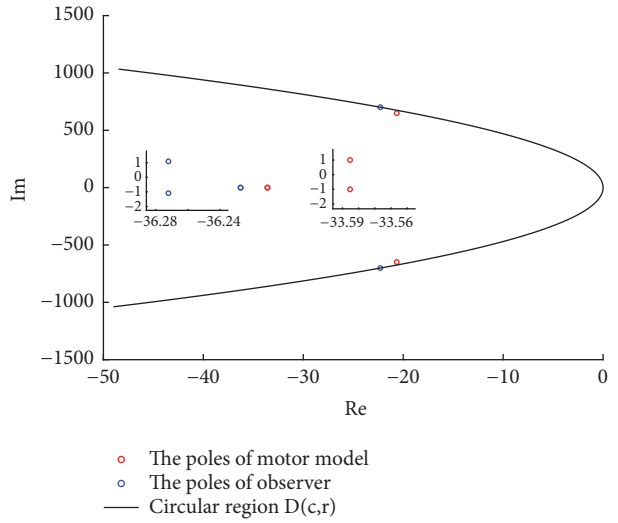

Figure 7: The poles of the motor model and observer.

$$\boldsymbol{G} = \begin{bmatrix} -0.0215 & 0.0008 \\ -0.0008 & 0.0215 \\ -2.3978 \times 10^{-5} & 2.8138 \times 10^{-6} \\ 2.8138 \times 10^{-6} & -2.3978 \times 10^{-5} \end{bmatrix}. \tag{57}$$

And then the train speed can be estimated by (55). Figure 8 displays the estimated result which indicates that the estimated speed can converge to real speed after 0.3s at each period, and the speed estimation system is stable. The error curve between real speed and estimated speed is shown in Figure 9; the max, min, and mean error value are given in Table 3. From Figure 9 and Table 3, we know that the proposed speed estimation law in this paper can estimate the train speed accurately; the mean error is less than 0.1m/s at each period. In addition, the max error is 2.32m/s and the error rate is 3.32% (the target speed is 70m/s at this period).

5.2. The Validity of NHMPM and Adaptive Parameter Estimation Algorithm. Figure 10 shows the estimated resistance

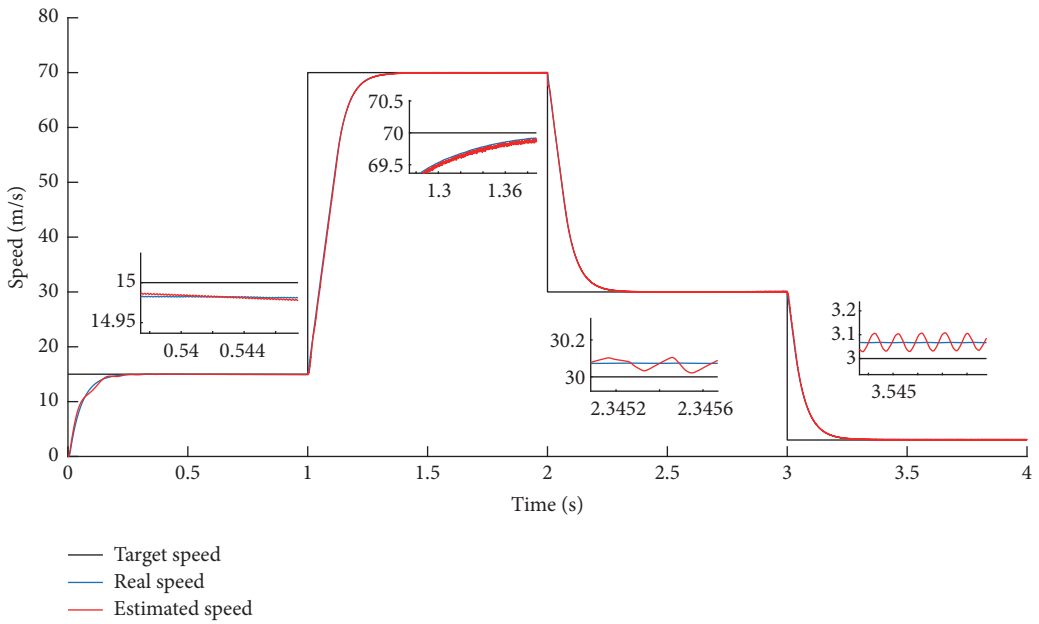

Figure 8: The estimated speed of the train.

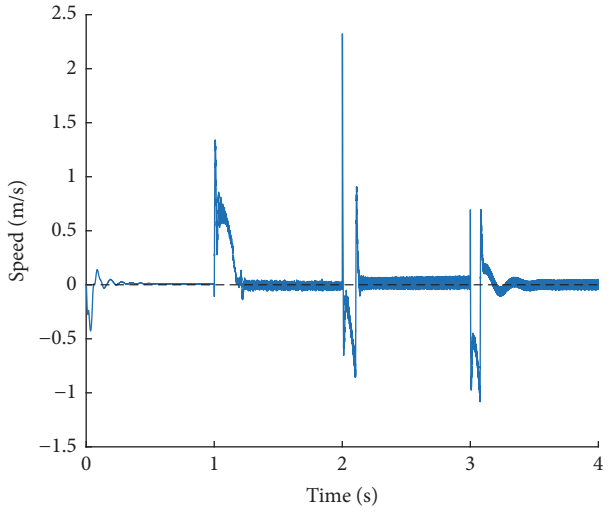

Figure 9: The error between real speed and estimated speed.

coefficients using the proposed adaptive parameter estimation algorithm. The unknown resistance parameters can converge to the real value accurately even when the real value changes from $c_0 = 0.42$, $c_v = 0.0016$, $c_a = 0.000132$ to $c_0 = 0.47$, $c_v = 0.0026$, $c_a = 0.001132$. It verifies the validity of the adaptive estimation algorithm.

Figure 11 and Table 4 show the verification results of NHMPM; it can be seen that the speed of NHMPM (green line) is basically consistent with the real speed that verifies the effectiveness of NHMPM. Moreover, compared with the TMPM, the NHMPM speed is closer to the real speed at the same traction and braking force. And the mean error between real speed and NHMPM speed is smaller than the mean error between real speed and TMPM speed at all periods especially at the periods of 2s-3s and 3s-4s, which indicates that NHMPM is more accurate than TMPM.

The traction motor stator voltage $u_{s\alpha}$, $u_{s\beta}$ and the electromagnetic torque of the first car are shown in Figures 12 and 13, respectively. Figure 14 displays the traction and braking force of three cars. As the second car is a carriage, its traction and braking force are zero. In contrast, the first and the third car are equipped with traction motor; therefore, they can supply traction and braking force in all modes.

6. Conclusions

This paper established a NHMPM including the integer variables of running status and car types for HST. As the basis

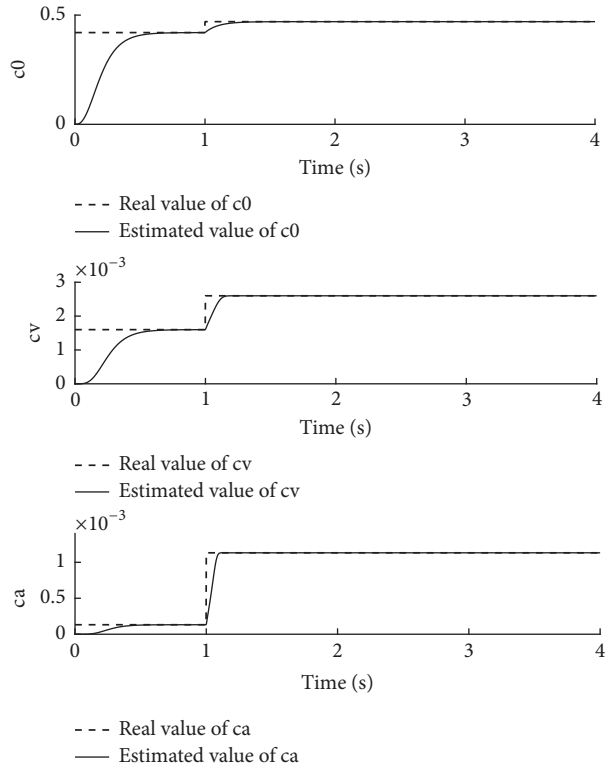

Figure 10: The estimated values of resistance coefficients.

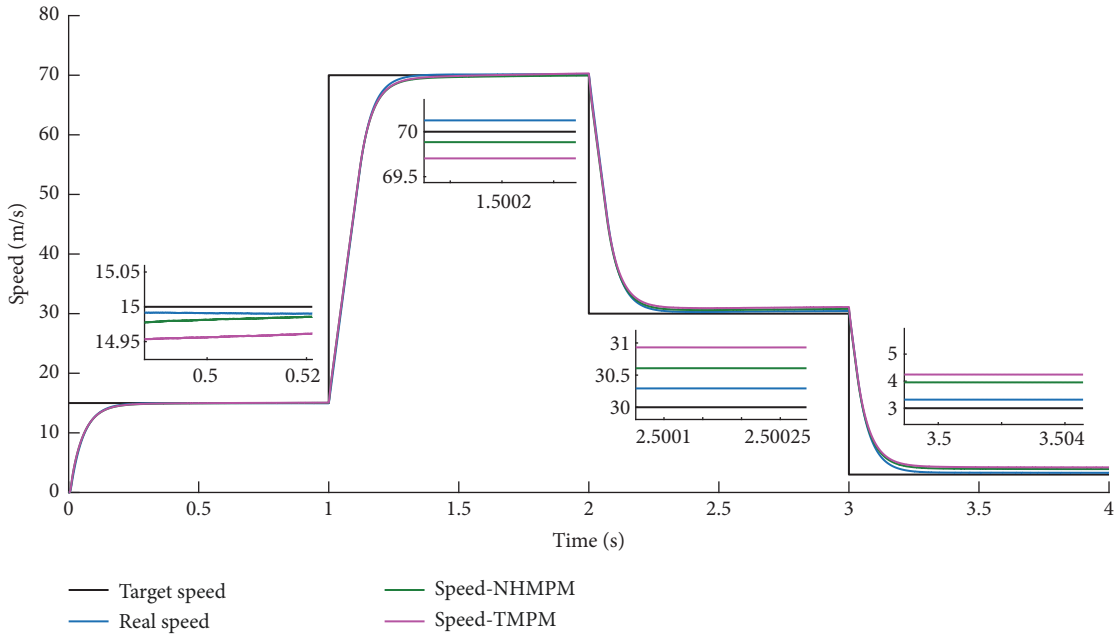

Figure 11: Train speed trajectory.

Table 3: The error value between real speed and estimated speed.

Value (m/s)	Period (s)			
	0s-1s	1s-2s	2s-3s	3s-4s
Max	0.1394	1.3407	2.3227	0.6965
Min	-0.4277	-0.1374	-0.8565	-1.0835
Mean	-0.0015	0.0910	-0.0128	-0.0378

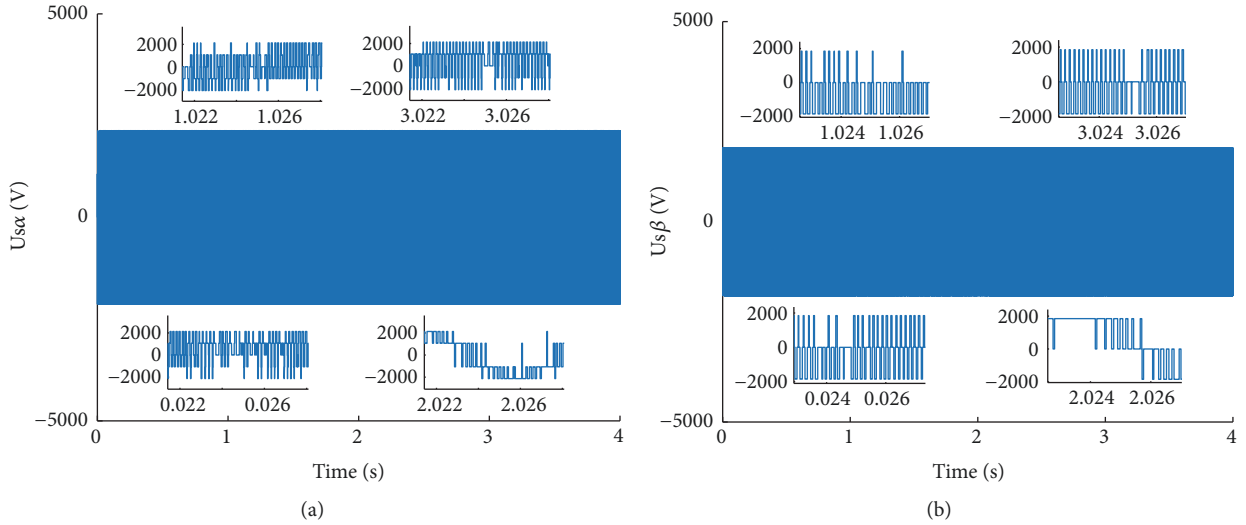

Figure 12: Traction motor stator voltage of the first car. (a) $u_{s\alpha}$, (b) $u_{s\beta}$.

Table 4: The max, min, and mean error between real speed and TMPM speed, real speed and NHMPM speed.

Period	0s-1s		1s-2s		2s-3s		3s-4s	
Value (m/s)	Types							
	TMPM	NHMPM	TMPM	NHMPM	TMPM	NHMPM	TMPM	NHMPM
Max	0.1561	0.1550	0. 6063	0. 5372	0.9741	0.6317	-0.1487	0.2647
Min	-0.5214	-0.5214	-0.7588	-0.7434	-0.8481	-0.4356	-1.2354	-0.8210
Mean	0.0763	0.0325	0.2871	0.2658	0.714	-0.2734	1.1202	-0.7064

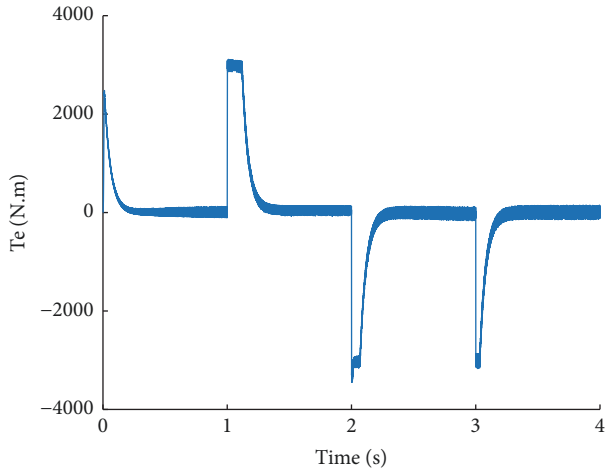

Figure 13: The traction motor electromagnetic torque of the first car.

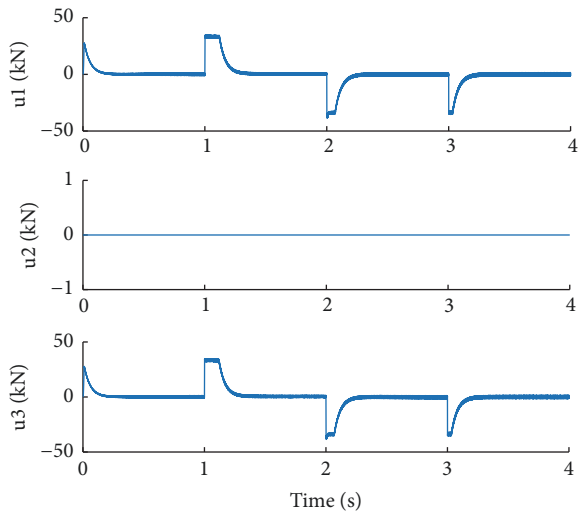

Figure 14: Traction and braking force of each car.

of research, the traction/braking dynamics was discussed and the running resistance force was reformulated. The author also analyzed the nonlinear in-train coupling force. Besides, an adaptive parameters estimation algorithm and a train speed estimation law were proposed. The proposed algorithm and law provide the unknown resistance coefficients and train speed required in the model, respectively. At last, numerical simulations are conducted to verify the effectiveness of the proposed algorithm, law, and NHMPM. The results of the verification are shown as follows. (1) The estimated speed using the proposed estimation law can converge to the real speed accurately. The mean error between real speed and estimated speed is less than 0.1m/s at each period, and the maximum error is 2.32m/s (the target speed is 70m/s at this period). (2) The estimated unknown resistance coefficients can converge to the real value accurately even when the real value changes. (3) The speed of NHMPM is basically

consistent with the real speed. Compared with TMPM, it is closer to the real speed at all periods especially at the periods of 2s-3s and 3s-4s.

Data Availability

The data used to support the findings of this study are included within the article.

Conflicts of Interest

The authors declare that there are no conflicts of interest regarding the publication of this paper.

Acknowledgments

This research was supported by the National Key R&D Program of China [2016YFB1200602-26]; the National Key R&D Program of China [2016YFB1200601]; the National Natural Science Foundation of China (Nos. U1734211).

References

[1] H. Dong, B. Ning, B. Cai, and Z. Hou, "Automatic train control system development and simulation for high-speed railways," *IEEE Circuits and Systems Magazine*, vol. 10, no. 2, pp. 6–18, 2010.

[2] L. J. Zhang and X. T. Zhuan, "Optimal operation of heavy-haul trains equipped with electronically controlled pneumatic brake systems using model predictive control methodology," *IEEE Transactions on Control Systems Technology*, vol. 22, no. 1, pp. 13–22, 2014.

[3] P. G. Howlett, P. J. Pudney, and X. Vu, "Local energy minimization in optimal train control," *Automatica*, vol. 45, no. 11, pp. 2692–2698, 2009.

[4] H. Luo, H. Xu, and X. Liu, "Immersion and invariance based robust adaptive control of high-speed train with guaranteed prescribed performance bounds," *Asian Journal of Control*, vol. 17, no. 6, pp. 2263–2276, 2015.

[5] R. S. Luo, Y. H. Wang, Z. Y. Yu et al., "Adaptive Stopping Control of Urban Rail Vehicle," *Journal of the China Railway Society*, vol. 34, no. 4, pp. 64–68, 2012 (Chinese).

[6] C. Yang and Y. Sun, "Robust cruise control of high speed train with hardening/softening nonlinear coupler," in *Proceedings of the American Control Conference (ACC '99)*, pp. 2200–2204, San Diego, Calif, USA, June 1999.

[7] B. Wie and D. S. Bernstein, "A benchmark problem for robust control design," in *Proceedings of the 1990 American Control Conference*, pp. 961-962, May 1990.

[8] C. Yang and Y. Sun, "Mixed H_2/H_∞ cruise controller design for high speed train," *International Journal of Control*, vol. 74, no. 9, pp. 905–920, 2001.

[9] M. Chou, X. Xia, and C. Kayser, "Modelling and model validation of heavy-haul trains equipped with electronically controlled pneumatic brake systems," *Control Engineering Practice*, vol. 15, no. 4, pp. 501–509, 2007.

[10] Q. Song, Y.-D. Song, T. Tang, and B. Ning, "Computationally inexpensive tracking control of high-speed trains with traction/braking saturation," *IEEE Transactions on Intelligent Transportation Systems*, vol. 12, no. 4, pp. 1116–1125, 2011.

[11] L. S. Wang, H. Z Xu, M. N. Zhang et al., "Hybrid Model Predictive Control Application to Automatic Train Operation," *Journal of the China Railway Society*, vol. 37, no. 12, pp. 53–60, 2015.

[12] Z.-Y. Yu and D.-W. Chen, "Modeling and system identification of the braking system of urban rail vehicles," *Journal of the China Railway Society*, vol. 33, no. 10, pp. 37–40, 2011.

[13] Q. Song, Y. D. Song, and W. Cai, "Adaptive backstepping control of train systems with traction/braking dynamics and uncertain resistive forces," *Vehicle System Dynamics: International Journal of Vehicle Mechanics and Mobility*, vol. 49, no. 9, pp. 1441–1454, 2011.

[14] Q. Song and Y. D. Song, "Robust and Adaptive Control of High Speed Train," in *Proceedings of Chinese Control and Decision Conference*, vol. 22, pp. 2469–2474, 2010.

[15] S. B. Yao, D. L. Guo, G. W. Yang et al., "Distribution of High-speed Train Aerodynamic Drag," *Journal of the China Railway Society*, vol. 34, no. 7, pp. 18–23, 2012.

[16] L. M. Song, *EMU Transmission and Control*, China Railway Publishing House, Beijing, China, 2009.

[17] J. Wang, W.-H. Gui, X.-H. Nian, and X.-F. Li, "Study on speed sensorless indirect stator-quantities control system of traction motor," *Journal of the China Railway Society*, vol. 32, no. 6, pp. 17–21, 2010.

[18] H. Kubota, K. Matsuse, and T. Nakano, "DSP-based speed adaptive flux observer of induction motor," *IEEE Transactions on Industry Applications*, vol. 29, no. 2, pp. 344–348, 1993.

[19] H. Kubota, I. Sato, Y. Tamura, K. Matsuse, H. Ohta, and Y. Hori, "Regenerating-mode low-speed operation of sensorless induction motor drive with adaptive observer," *IEEE Transactions on Industry Applications*, vol. 38, no. 4, pp. 1081–1086, 2002.

[20] G. Yang and T. Chin, "Adaptive-speed identification scheme for a vector-controlled speed sensorless inverter-induction motor drive," *IEEE Transactions on Industry Applications*, vol. 29, no. 4, pp. 820–825, 1993.

[21] S. Suwankawin and S. Sangwongwanich, "A speed-sensorless IM drive with decoupling control and stability analysis of speed estimation," *IEEE Transactions on Industrial Electronics*, vol. 49, no. 2, pp. 444–455, 2002.

[22] S. Suwankawin and S. Sangwongwanich, "Design strategy of an adaptive full-order observer for speed-sensorless induction-motor drives - Tracking performance and stabilization," *IEEE Transactions on Industrial Electronics*, vol. 53, no. 1, pp. 96–119, 2006.

[23] M. Liu, Y. Jing, and S. Zhang, "Robust state observer design based on regional pole assignment," *International Federation of Automatic Control*, vol. 38, pp. 1263–1268, 2005.

[24] S. Q. Zhao, Y. F. Ma, and X. P. Gu, "Comparative and analysis of regional poles in the robotic arm movement model," *Computing Technology and Automation*, vol. 31, no. 4, pp. 21–25, 2012.

[25] K. Y. Guo, F. Z. Wang, and B. Sun, "Uniform damping control of low-frequency oscillations in power systems based on region poles assignment," *Transactions of China electrotechnical Society*, vol. 24, no. 12, pp. 142–148, 2009.

[26] J. Wang, W. H. Wu, J. T. Liu et al., "H_2/H_∞ control with regional pole placement for carrier landing," *Computer Simulation*, vol. 34, no. 12, pp. 41–44, 2017.

[27] Z. H. Li, C. J. Chen, J. Teng et al., "Application of State Feedback Control based on Regional Pole-Assignment Method in Flexible Buildings," *Journal of Vibration Engeering*, vol. 31, no. 2, pp. 265–274, 2018.

[28] L. Yu, *Robust Control-LMI Approach*, Tsinghua University Press, Beijing, China, 2002.

[29] V. Adetola, D. Dehaan, and M. Guay, "Adaptive model predictive control for constrained nonlinear systems," *Systems & Control Letters*, vol. 58, no. 5, pp. 320–326, 2009.

[30] Z. Rao, *Train traction calculation*, China Railway Publishing House, Beijing, china, 2012.

[31] C. B. Zhang and Y. P. Tang, "Research and Simulation on Effect of Gear Ratio on High-Speed EMU Tractive Characterisation," *Journal of Dalian Jiaotong University*, vol. 4, pp. 79–82, 2011.